

Genetically-Optimized Electromagnetic Bandgap Structures for Efficient 5G Implementations

Dimitrios Karatzidis, Anestis Apostolidis, Stamatios Amanatiadis, and Nikolaos Kantartzis

Department of Electrical and Computer Engineering

Aristotle University of Thessaloniki

Thessaloniki, Greece

{karatzidis,samanati,kant}@ece.auth.gr

Abstract—In this paper, we employ a systematic and accurate genetic optimization methodology, which incorporates a fast finite-element solver, in order to derive prototype electromagnetic bandgap structures with the maximum possible bandgap or multiple bandgap operational regions. All simulation results are, also, extracted by means of a commercial computational package, verifying thus the advantages of the technique. Finally, a realistic case as part of a 5G telecommunications scenario is examined, where one of the prototype geometries, so developed, is set as ground plane of a printed $\lambda/2$ dipole antenna.

Index Terms—Computational electromagnetics, dispersion diagram, electromagnetic bandgap, optimization.

I. INTRODUCTION

Since their initial advent, planar structures have gained a constantly growing interest. The implementation of such devices in the microwave regime is based on a periodic arrangement of metallic elements atop a flat surface, which achieves a band gap for surface waves or, in other words, a high surface impedance within the restricted frequency band. Essentially, this high impedance surface is a kind of two-dimensional photonic crystal that prevents the propagation of surface currents within the band gap in the radio-frequency and microwave spectrum. Moreover, when electromagnetic bandgap (EBG) devices are used as ground planes, they can lead to a large gain increase of the resulting printed antennas [1]–[6]. Thus, being capable of controlling the wave propagation, EBG structures may suppress unwanted leakage in microwave integrated circuits and drastically improve the overall efficiency of microstrip antennas [7]–[13].

The bandgap information of an EBG device, as the main element of an integrated microwave circuit, is of major importance from the design point of view. If the dimensions of the device are small compared to the wavelength, its electromagnetic properties can be described in terms of the active medium theory. The model of an active surface impedance, actually, summarizes the properties of the surface in a simple parameter, namely the surface impedance. It can predict the reflection properties and several attributes of the surface waves that form the band gap, but not the band gap itself, which, by definition, must extend over large wave vectors. A complete electromagnetic analysis is, therefore, required to obtain the dispersion diagram and since no analytical approach is available, the numerical modelling seems to be the most attractive candidate [14]–[16].

Considering these facts, it is the objective of this paper to profitably use a genetic optimization algorithm, based on the finite element concept, in an effort to design advanced EBGs with fully reconfigurable properties. After introducing the appropriate cost function, the technique performs the necessary simulations and provides the optimized EBG form, which best fits to the design requirements. Computational results, derived through a popular computational package, prove the accuracy of our method which yields very interesting outcomes. The verification concludes with a real-world 5G application of a printed $\lambda/2$ dipole antenna, whose ground plane comprises an EBG geometry obtained with the aid of the prior algorithm.

II. DEVELOPMENT OF THE PROTOTYPE EBG STRUCTURES

Firstly, a genetic algorithm combined with the prism macroelement method, thoroughly described in [16], is employed to pursue the ideal EBG configuration. To this aim, we develop a very fast technique for the desired bandgap construction of our EBG devices, which in their two-dimensional rendition are formed by pixels. Then, by exploiting the smooth integration of macroelements in evolutionary optimization processes [16], the prototype EBG devices are carefully designed. In essence, the latter are derived after a large number of optimizations, under the condition of the maximum possible bandwidth for all wave vectors. Explicitly, the optimization intends to maximize the relative size of the bandgap between zones 1 and 2 of the dispersion diagram, i.e. to maximize the minimum value of zone 2 and concurrently minimize the maximum value of zone 1. This, in fact, constitutes the key difference of the proposed cost function, F , compared to existing works. Consequently, we define

$$F = \min_i \omega_2^i(\mathbf{k}) - \max_i \omega_1^i(\mathbf{k}), \quad (1)$$

where $\omega_j^i(\mathbf{k})$ are the i frequencies of zone j , for $j = 1, 2$. As observed, (1) can be deemed adequately sophisticated in the sense that it precisely represents a problem of many variables, namely the \mathbf{k} wave vectors, whose eigenfrequencies vary during the optimization procedure. Since during each step of the algorithm, only the eigenvalue search routine affects the computational overhead, seven wave vectors are proven sufficient to accurately represent the \mathbf{k} -space for the evaluation of the cost function.

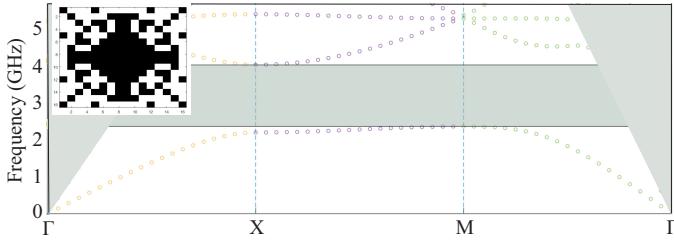


Fig. 1. Dispersion diagram for the geometry of the first proposed structure (inset sketch: black pixels denote metal and white pixels denote dielectric).

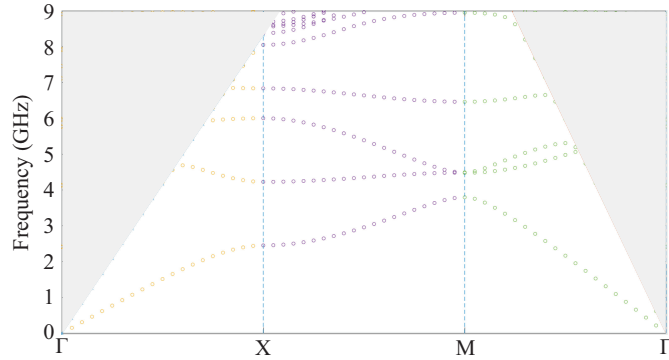


Fig. 2. Dispersion diagram for the structure of Figure 1, with a slightly increased unit cell size. Note that the original bandgap has totally disappeared.

In this framework, starting with random designs, assuming a small (or even no) bandgap, and without any other *a priori* information, our optimization process results in the design shown in the inset of Figure 1. Note that black pixels correspond to the presence of metal, while the white ones suggest the presence of dielectric medium. The only constants are: the unit cell size, set equal to 18 mm, and the dielectric medium, chosen to be FR4 ($\epsilon_r = 4.5$), with a thickness of $h = 1.5$ mm. The dispersion diagram of Figure 1 exhibits a $\Delta f = 1.68$ GHz bandwidth at the central frequency $f_0 = 3.16$ GHz, with a bandgap-to-midgap ratio $\Delta f/f_0 = 0.5316$ or 53.16%.

A remarkable result, however, is obtained if we increase the unit cell size by 1 mm, while maintaining the same pattern dimensions. Indeed, the dispersion diagram of Figure 2 reveals that the original bandgap has been completely eliminated, and its place is, now, occupied by three smaller bandgaps with central frequencies well above that of the initial geometry, given in Figure 1. Furthermore, the bandgap-to-midgap ratio for each of these bandgaps is drastically decreased, thus certifying that the aforementioned modification offers an extra degree of freedom to adjust the operating frequency of the structure under design. In other words, while for the initial geometry, we were limited between 2.3 and 4 GHz, the increased unit cell leads to ranges around 4.5, 5.5 or even up to 6 GHz. It becomes apparent, though, that the new bandwidth is smaller than the initial one, yet such frequency specifications are very popular in a large assortment of contemporary 5G implementations.

Next, we examine the optimized high-impedance EBG prototype, depicted in the inset of Figure 3, which provides

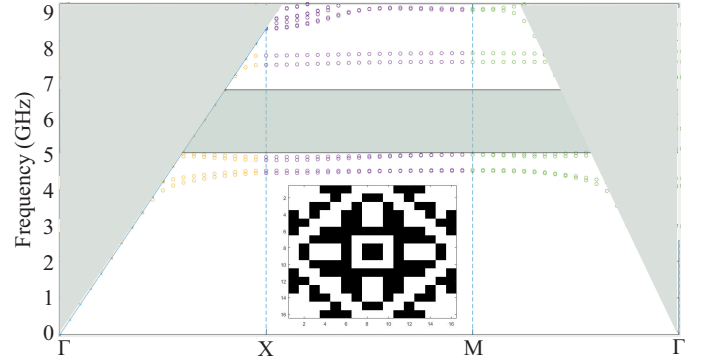


Fig. 3. Dispersion diagram for the EBG prototype of the inset sketch (black pixels denote metal and white pixels denote dielectric) with a bandgap at a higher central frequency.

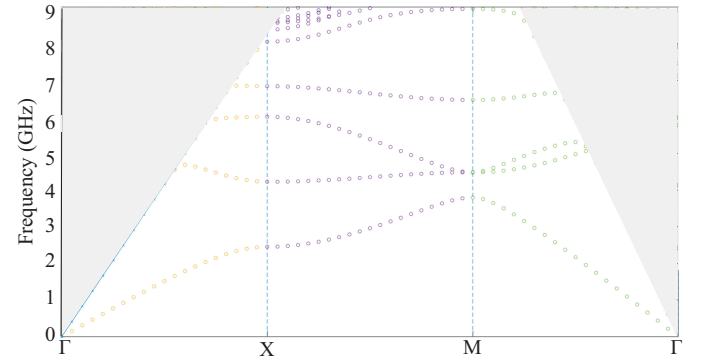


Fig. 4. Dispersion diagram for the complementary structure of the first EBG prototype, depicted in Figure 1.

a bandgap at a much higher central frequency. Actually, one can discern that this bandgap is fairly large, as the one in Figure 1, yet at a completely different frequency range. More specifically, we acquire a $\Delta f = 1.7$ GHz bandwidth at the central frequency $f_0 = 5.75$ GHz, as given in Figure 3, with a bandgap-to-midgap ratio $\Delta f/f_0 = 0.2956$ or 29.56%.

Probing further, it is noteworthy to study the complementary geometries of the above structures with the same unit cell size. Our motive stems from the concept of frequency selective surfaces (FSS). It is well-known that if an FSS exhibits a bandpass behaviour at a specific frequency range, its complementary geometry will present bandstop features at the same spectrum. Therefore, we investigate whether an analogous performance holds for the proposed EBG surfaces, i.e. the appearance of a bandgap outside the frequency range of the original structure. Hence, Figure 4 presents the dispersion diagram of the complementary geometry of the first EBG surface (see Figure 1), where it is observed that although the initial bandgap has actually disappeared, two new bandgaps (of smaller bandwidth) emerge approximately at 3.9 and 6.5 GHz. This interesting outcome unveils that the complementary structure is probably of limited use in the case of EBG designs for 5G realizations. Similar conclusions are drawn from the dispersion diagram of Figure 5 for the complementary structure of the second EBG design, given in Figure 3.

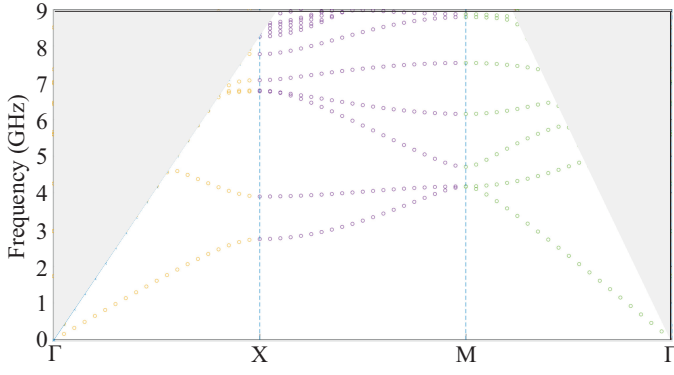


Fig. 5. Dispersion diagram for the complementary structure of the second EBG prototype, described in Figure 3.

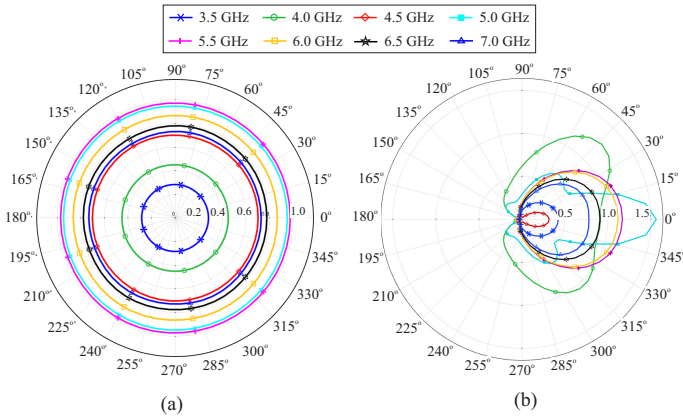


Fig. 6. Radiation patterns of a printed $\lambda/2$ dipole antenna (a) in the absence of a ground plane and (b) in the presence of a 5×5 unit-cell EBG ground plane at a distance of $\lambda_0/20$ from the dipole. The frequency range varies from 3.5 to 7 GHz with an increment of 0.5 GHz.

III. EBG DESIGNS FOR ANTENNA GROUND PLANES

To verify the efficiency of the featured EBG designs, we study a realistic scenario in which these prototype structures are utilized as ground planes for a printed $\lambda/2$ dipole antenna. For this purpose, all of our simulations are conducted by means of COMSOL Multiphysics computational package [17], where the antenna along with the EBG-based ground plane are appropriately modeled. It should be stressed that a central frequency shift and, particularly, a bandgap width modification is to be anticipated, since our EBG geometry is, now, finite.

Based on these aspects, we select the high-frequency EBG surface of Figure 3, whereas the dipole is designed to operate approximately at 6 GHz, in order to radiate effectively within the theoretically predicted bandgap. Our analysis focuses on the behavior of the antenna radiation pattern by varying the EBG ground plane size from 5×5 to 9×9 unit cells. In this manner, we attempt to certify whether the operational bandwidth of the ground plane increases and the theoretical dispersion diagram of Figure 3 is approached. As a reference, and starting from the 5×5 case, we consider the radiation pattern of the $\lambda/2$ dipole in the absence of a ground plane, presented in Figure 6(a). Initially, the device is characterized over

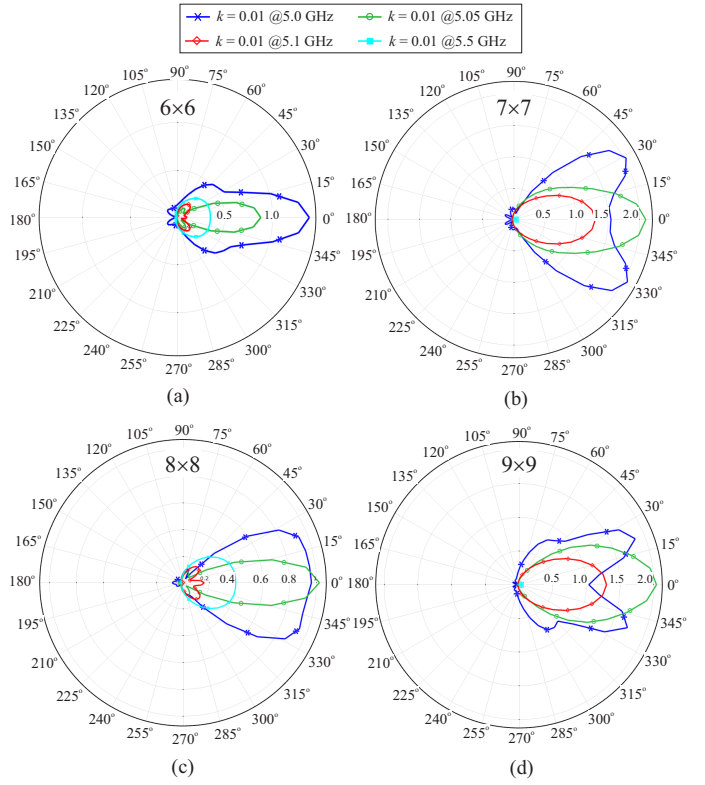


Fig. 7. Radiation patterns at specific frequencies of a dipole antenna with an EBG-based (via the design of Figure 3) ground plane and a unit cell size of: (a) 6×6 , (b) 7×7 , (c) 8×8 , and (d) 9×9 . The distance between the antenna and the ground plane is $\lambda_0/100$.

the relatively wide frequency range from 3.5 to 7 GHz with a step of 0.5 GHz, in order to detect the optimal operational frequency. As determined below, this frequency is found to be $f_0 = 5.05$ GHz, and thus all radiation patterns are extracted for the respective central wavelength of $\lambda_0 = 5.94$ cm. Moreover, the distance between the antenna and the EBG ground plane varies, also, from $\lambda_0/100$ to $\lambda_0/4$, with the optimal distance obtained at $\lambda_0/20$ for an array of 5×5 unit cells. The derived radiation patterns, given in Figure 6(b), indicate the promising improvement of the antenna directivity due to the proposed EBG-based ground plane at 5 GHz, which is, actually, within the theoretically obtained bandgap.

Subsequently, concentrating on 5 GHz, we examine if an increase of the unit cell dimensions, extends the EBG structure bandwidth, as well. Therefore, the size augments from 5×5 to 9×9 , while the antenna-ground distance is set to $\lambda_0/100$. The study is conducted in the frequency spectrum between 4.9 and 5.5 GHz, however only some characteristic values are selected to present the overall behavior. As detected from Figure 7, the resulting radiation patterns do not exhibit a significant improvement at approximately 5.05 GHz; implying that despite the increased number of unit cells, the bandwidth is not seriously affected. Another notable observation is that the radiation patterns become better (i.e. more directive) in the case of even unit-cell numbers, probably owing to the

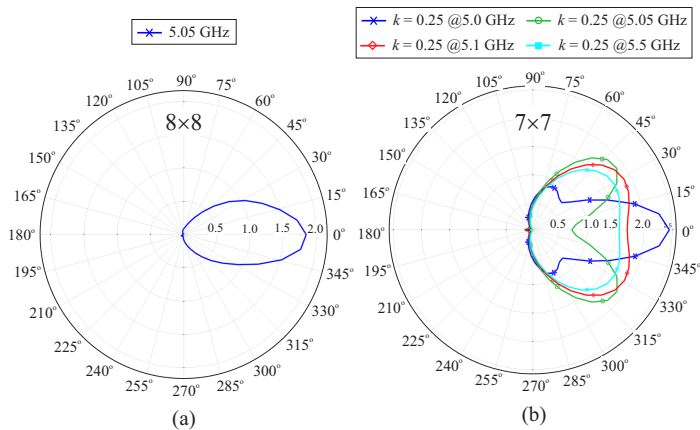


Fig. 8. Radiation patterns of a dipole with (a) an 8×8 EBG ground plane at a distance of $\lambda_0/100$, shifted by half a grid constant at 5.05 GHz and (b) a 7×7 EBG ground plane at a distance of $\lambda_0/4$ and different frequencies.

symmetry that affects the device performance. To confirm this assumption, we shift the dipole by half a grid constant and conduct new simulations with the outcomes shown in Figure 8(a). Apart from the obvious radiation pattern improvement, we also detect a rotation of the central lobe; a fact which is expected, since the ground plane is not symmetrically placed with respect to the dipole. Despite this improvement, nonetheless, the pattern is still inferior to that of the 7×7 implementation. In addition, we can safely conclude that the EBG surface operates efficiently within a small bandwidth around 5.05 GHz for odd unit cell numbers. Finally, Figure 8(b) confirms that the radiation pattern degrades at 5.05 GHz in the case of large distances from the ground plane, e.g. $\lambda_0/4$.

IV. CONCLUSION

An accurate genetic optimization technique has been presented in this paper for the design of enhanced EBG structures. Based on a new cost function and a rapid finite-element analysis, the proposed structures have been comprehensively investigated and applied to real-world antenna configurations for 5G scenarios. Summarizing our findings, it is concluded that for a finite-sized EBG ground plane, the unit cell size can not seriously increase the operational frequency range. On the other hand, results indicate that the relative dipole-ground plane distance can strongly affect the radiation pattern of the device. Moreover, the symmetric establishment of the antenna relative to the grid center leads to the best performance, considering an odd number of cell elements. Since the specific

analysis refers only to the case of a printed $\lambda/2$ dipole antenna, future work intends to extend the featured method to more complex radiators and diverse ground-plane arrangements.

REFERENCES

- [1] H. Malekpoor and S. Jam, "Improved radiation performance of low profile printed slot antenna using wideband planar AMC surface," *IEEE Trans. Antennas Propag.*, vol. 64, no. 11, pp. 4626-4638, Nov. 2016.
- [2] M. Mantash and T. A. Denidni, "CP antenna array with switching-beam capability using electromagnetic periodic structures for 5G applications," *IEEE Access*, vol. 7, pp. 26192-26199, 2019.
- [3] S. Ullah, W.-H. Yeo, H. Kim, and H. Yoo, "Development of 60-GHz millimeter wave, electromagnetic bandgap ground planes for multiple-input multiple-output antenna applications," *Sci. Rep.*, vol. 10, art. no. 8541, pp. 1-12, 2020.
- [4] S. Modak, T. Khan, and R. H. Laskar, "Penta-notched UWB monopole antenna using EBG structures and fork-shaped slots," *Radio Sci.*, vol. 55, no. 9, pp. 1-11, Sept. 2020.
- [5] B. P. Smith and A. K. Iyer, "Low-profile uniplanar dual-band and dual-polarized microstrip patch antenna using embedded MTM-EBGs," *IEEE Trans. Antennas Propag.*, vol. 69, no. 7, pp. 3645-3653, July 2021.
- [6] V. Jandieri, S. Ceccuzzi, P. Baccarelli, G. Schettini, D. Erni, W. Hong, D. H. Werner, and K. Yasumoto, "Efficient analysis of radiation from a dipole source in woodpile EBG structures," *IEEE Trans. Antennas Propag.*, vol. 70, no. 1, pp. 389-400, Jan. 2022.
- [7] D. Chen, W. Yang, and W. Che, "High-gain patch antenna based on cylindrically projected EBG planes," *IEEE Antennas Wireless Propag. Lett.*, vol. 17, no. 12, 2374-2378, Dec. 2018.
- [8] Y. Alnaiemy and L. Nagy, "Improved antenna gain and efficiency using novel EBG layer," in *Proc. 2020 IEEE 15th Int. Conf. Syst. Syst. Engr. (SoSE)*, Budapest, Hungary, 2020, pp. 271-276.
- [9] C. Máximo-Gutiérrez, J. Hinojosa, F. L. Martínez-Viviente, and A. Alvarez-Melcon, "Design of high-performance microstrip and coplanar low-pass filters based on electromagnetic bandgap (EBG) structures," *AEU - Int. J. Electron. Commun.*, vol. 123, art. no. 153311, 2020.
- [10] R. Pei, M. P. Leach, E. G. Lim, Z. Wang, C. Song, J. Wang, W. Zhang, Z. Jiang, and Y. Huang, "Wearable EBG-backed belt antenna for smart on-body applications," *IEEE Trans. Industr. Inform.*, vol. 16, no. 11, pp. 7177-7189, Nov. 2020.
- [11] A. Khan, S. Bashir, S. Ghafoor, and K. K. Qureshi, "Mutual coupling reduction using ground stub and EBG in a compact wideband MIMO-antenna," *IEEE Access*, vol. 9, pp. 40972-40979, 2021.
- [12] S. Dey and S. Dey, "Broadband high gain cavity resonator antenna using planar electromagnetic bandgap (EBG) superstrate," *Int. J. Microw. Wireless Technol.*, 1-12, 2022.
- [13] H.-K. Nie, X.-W. Xuan, Q. Shi, A. Guo, M.-J. Li, H.-J. Li, and G.-J. Ren, "Wearable antenna sensor based on EBG structure for cervical curvature monitoring," *IEEE Sensors J.*, vol. 22, no. 1, pp. 315-322, Jan. 2022.
- [14] B. Li, Y. Wang, C. Xuan, and K. Yan, "Constructal optimization of power distribution networks for electromagnetic bandgap power plane using the generative design algorithm," *IEEE Trans. Electromagn. Compat.*, vol. 62, no. 2, pp. 549-560, Apr. 2020.
- [15] R. Sravya and R. Kumari, "Gain and isolation enhancement of patch antenna using L-slotted mushroom electromagnetic bandgap," *Int. J. Rf Microw. Comput.-Aided Engr.*, vol. 30, no. 10, 2020.
- [16] D. I. Karatzidis, N. V. Kantartzis, G. G. Pyrialakos, T. V. Yioultis, and C. S. Antonopoulos, "Genetic optimization with mixed-order prism macroelements for 3-D metamaterial multilayered structures," *IEEE Trans. Magn.*, vol. 55, no. 6, art. no. 7203904, pp. 1-4, June 2019.
- [17] COMSOL Multiphysics®, *COMSOL AB*, Stockholm, Sweden, 2019.